

Electrochemical Performance of Co₃O₄ Nanofibers As Anode Material for Lithium-Ion Batteries

Jianfeng Dai^{a,b,*}, Xiaojun Zhu^b, Jifei Liu^a, Qing Wang^{a,b}, Weixue Li^{a,b}, and Yufeng Qi^b

^aState Key Laboratory of Advanced Processing and Recycling of Non-ferrous Metals, Lanzhou University of Technology, Lanzhou, Gansu, 730050 PR China

^bSchool of Science, Lanzhou University of Technology, Lanzhou, Gansu, 730050 PR China

*e-mail: daijf@lut.cn

Received June 28, 2018; revised June 28, 2018; accepted September 15, 2018

Abstract—Nanostructuring is a promising approach to the problems of low diffusion coefficient of transition metal oxides anodes. Co₃O₄ nanofibers electrode materials were successfully synthesized by electrospinning followed by controlled pyrolysis. Electrode materials based on Co₃O₄ nanofibers applied as anode for lithium-ion batteries (LIBs) show high discharge-charge specific capacity of 595 and 527 mA h g⁻¹ at 0.5C, respectively. Further electrochemical investigation reveals that Co₃O₄ nanofibers exhibiting high specific capacity (300 mA h g⁻¹ at 0.5C after 200 cycles), the capacity fading is only 11.8% after 200 cycles. Further electrochemical studies reveal that these excellent electrochemical properties should be attribute to the ordered ions diffusion pathway originated from the one-dimensional nanostructure and continuous fibrous network structure. These results revealed that the Co₃O₄ nanofibers are promising anode materials for LIBs.

Keywords: Co₃O₄, anode material, nanofibers, electrospinning

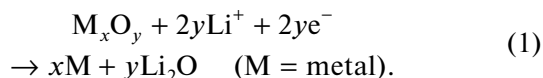
DOI: 10.1134/S0036024419100054

1. INTRODUCTION

The search for high energy densities, excellent cyclic stability, and environmentally friendly materials is a key to energy saving in energy storage and electric vehicles, which results in a lower carbon footprint. Safe, low cost, and high rate capability LIBs are required for the future devices [1]. As performance of LIBs is largely dependent on the electrode materials, the design and fabrication of novel electrode materials have attracted considerable attention [2]. Nevertheless, the capacities of commercial electrodes are far from sufficient, i.e., graphite anode with a theoretical capacity of 372 mA h g⁻¹ [3], which is hard to meet the high capability demand of LIBs for electric vehicles [4, 5]. With the increasing demand for higher energy densities LIBs, it is essential to find anodes with high theoretical specific capacity, excellent cycling performance, and good rate capability. On this basis, the novel anode material has attracted the extensive attention of researchers [6].

As an ordinary course, graphene, a single atomic layer of graphite, has been experimented in a variety of applications [7–10]. However, graphene has poor cyclability, high price as well as complicated preparation process limit its development in the anode materials for lithium-ion batteries. There other anode materials with high theoretical specific capacity for LIBs should be developed. Transition metal oxides

(TMOs) (such as Fe₃O₄, NiO, Mn₂O₃, and Co₃O₄) have been used as candidates of anode materials for LIBs due to high theoretical, and relatively low electrode potential versus Li/Li⁺ [11, 12]. Among anode materials, the theoretical capacity of transition metal oxides well above conventional anode material of graphite with low theoretical capacity [13–15]. The reaction between lithium and transition metal oxides based anodes is the so-called ‘conversion reaction’ reported in Eq. (1) [16]



Among TMOs, Co₃O₄ have been explored as promising anode materials for LIBs because of their high theoretical capacity, compared with graphite [17, 18]. Co₃O₄ particles with different morphologies like nanospheres and microflowers, have been synthesized and their electrochemical properties in lithium ion batteries have been investigated [19, 20]. However, these Co₃O₄ materials usually suffer from the problems of poor electronic conduction and severe volume change [21]. The Co₃O₄ nanofibers could achieve richer redox kinetics to reduce capacity loss during cycling [22]. The loading of Co₃O₄ nanometer material as an anode for LIBs has been reported by many

groups. Xin et al. [23] and Zhang et al. [24] reported that the Co_3O_4 material has exceedingly fine performance as anode material for LIBs.

One-dimensional nanostructure materials such as nanoneedles, nanowires and nanorods, are increasingly interesting due to their physicochemical properties and secondary batteries [25]. In this study, Co_3O_4 nanofibers were prepared by electrospinning, which is not only attributed to the improved diffusion kinetics caused by the ultralong and continuous one-dimensional fibrous structure, but also because increased ion transmission rate. It can be used as a substitute for mass production of carbon materials, in order to increase the capacity of lithium-ion batteries. Thus, the Co_3O_4 nanofibers are remarkable anode material for LIBs.

2. EXPERIMENTAL

2.1. Materials

Cobalt nitrate hexahydrate ($\text{Co}(\text{NO}_3)_2 \cdot 6\text{H}_2\text{O}$, Guangdong Guanghua Sci. Tech. Co. Ltd.) is used to manufacture cobalt (II, III) oxide. Polyvinylidene fluoride (PVDF, Aladdin Industrial Corporation) is used as a binder for the active substance to adhere to copper foil. N-Methyl-2-pyrrolidone (NMP, Aladdin Industrial Corporation) is used to mix active substances, acetylene black and PVDF. Acetylene black (Aladdin Industrial Corporation) is used as a conductive additive. N-Polyvinylpyrrolidone (PVP, Shanghai Zhong Qin chemical reagent co. LTD) is used as a binder in Co_3O_4 synthesis. *N,N*-Dimethylformamide (DMF, Aladdin Industrial Corporation) is used as a solvent to dissolve inorganic salts.

2.2. Experimental Detail

1.5 g of $\text{Co}(\text{NO}_3)_2 \cdot 6\text{H}_2\text{O}$ was dissolved in a 3 : 2 mixture of DMF and ethanol solution (a total of 5 mL). Next, 2 g of PVP (K30, $M = 10000$) was added to $\text{Co}(\text{NO}_3)_2 \cdot 6\text{H}_2\text{O}$ solution in order to increase the tackiness. The obtained precursor solution was transferred into a 5-mL glass syringe coupled with a 22-gauge stainless steel needle. The distance between the needle tip and collector (aluminum foil) was 20 cm. The applied voltage was 16 kV. The precursor nanofiber was dried at 60°C for 12 h in drying cabinet, finally calcined at 500°C for 4 h in tube furnace.

2.3. Characterization

The morphologies and microstructures were obtained using a JSM-6701F scanning electron microscope (SEM) at an acceleration voltage of 20 kV, which was fabricated using Japan Electronics Optical

Corporation. The crystal structure of the samples was characterized by powder X-ray diffraction (XRD) with Bruker D8 Advance using $\text{CuK}\alpha$ radiation within the 2θ range of 10° – 90° .

2.4. Electrochemistry

Electrochemical properties of the active substance were tested by using coin cells (CR2025). Working electrodes were manufacture by mixing and grinding the active materials, acetylene black and PVDF at a ratio weight of 8 : 1 : 1. Next, we add NMP to the above mixture to obtain viscous paste. Then, it was evenly coated on a copper foil, and subsequently dried at 80°C for 12 h in vacuum drying cabinet. Finally, the electrodes were assembled in a button cell in an argon-filled glove box. The CV was measured using a Wuhan Corrtest electrochemical workstation at a scan rate of 0.1 mV s^{-1} in the voltage range of ~ 0.01 – 3.0 V . The galvanostatic charge/discharge was performed on a LAND-CT2001A battery testing system. EIS measurements were performed with an Wuhan Corrtest electrochemical workstation within a frequency range of 0.01 Hz to 1000 kHz at a voltage amplitude of 4 mV.

3. RESULT AND DISCUSSION

Figure 1a shows the scheme of the electrospinning setup. The spinning process was conducted at 16 kV with a 20 cm gap between the needle tip and collector. It is made up of direct-current power supply, infusion pump and downtank. There are also some other things like power supply and electric motors. High voltage is used to introduce the static charge into the polymer solution or melt. The charged liquid is placed in a strong electrostatic field. The electrostatic repulsion drives the polymer solution to stretch and divide. Then it is solidified by evaporation or cooling of the solvent. Eventually, one can obtain fibers that reach the nanometer scale. Figure 1b shows the XRD patterns of Co_3O_4 nanofibers. The crystal structure were characterized by XRD in the range of 10° – 90° by step scanning. For the composites sample, the prominent diffraction peaks at 19.1° , 31.2° , 36.8° , 45.1° , 59.5° , and 65.3° are ascribed to the planes of Co_3O_4 (JCPDS 47-1049), which were indexed as the (111), (220), (311), (440), (511), and (440) crystal planes, respectively. The high peak intensity of all samples clearly confirmed their high crystallinity. No characteristic peaks from precursor impurities are detected.

Figure 2a shows the SEM image of nanofibers of the cobalt oxide precursor at $\times 10000$ magnification, which has not been calcined. The fibers are ~ 200 – 300 nm in diameter. Its main component is cobalt nitrate and PVP. Different types of needles can be used to change the diameter of the nanofibers. Figures 2b, 2c shows the morphology of Co_3O_4 nanofibers at different magnification after calcination. The diameter of

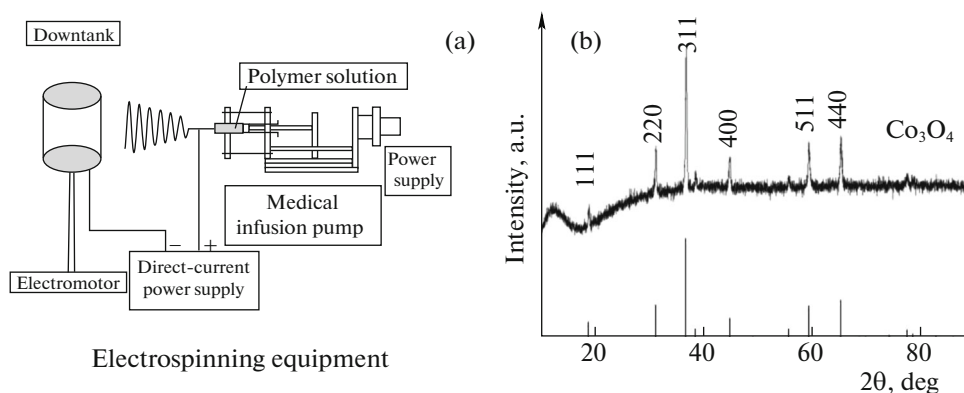


Fig. 1. (a) Simple device for electrostatic spinning; (b) XRD pattern of the Co_3O_4 nanofibers.

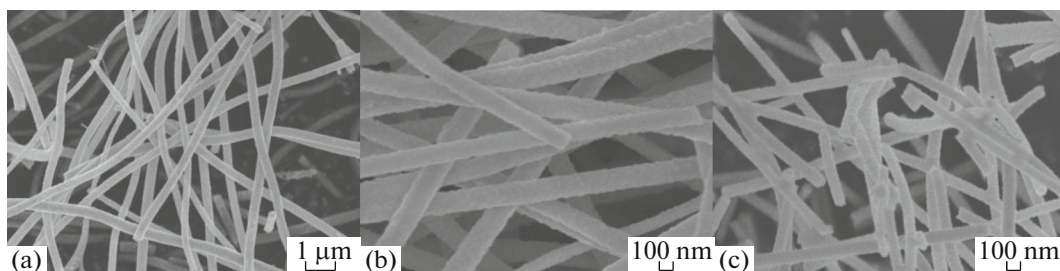


Fig. 2. (a) SEM diagram of nanofibers of the cobalt oxide precursor; (b, c) show the morphology of Co_3O_4 nanofibers after calcination.

the nanofibers is about $\sim 120\text{--}170$ nm. These nanofibers are pure Co_3O_4 .

Button batteries were assembled to test the performance of the Co_3O_4 nanofibers as anode materials. The first three CV curves of the Co_3O_4 nanofibers are shown in Figs. 3a, 3b. Figure 3a shows the new battery CV testing at the scan rate of 0.5 mV s^{-1} . During the first negative scan, a weak reduction peak appeared at 1.35 V, but it disappeared at the second scan and third scans, indicating an irreversible electrochemical reaction. This is primary attributed to the formation of solid electrolyte interface (SEI) caused by the decomposition of electrolyte [26]. The formation of SEI by the reaction with the electrolyte corresponds to a peak at 1.35 V. Another peak at 0.33 V is attributed to Co_3O_4 reduction to Co as well as the formation of Li_2O . The reaction equation is shown in (2). During the reverse positive scan, the oxidation peak emerged at 1.20 V, which corresponds to the conversion reaction of Co oxidized to Co_3O_4 . The reaction equation is shown in (3). Equation (4) is overall reaction equation. In the subsequent cycles, the peaks at 1.35 V disappear, the CV curves show a reduction peak at 0.33 V and a increment at 1.20 V, both of which keep stable in their forms and intensities, implying the activation process mainly occurred during the first discharge process. This redox

peaks in CV curves correspond to the following reactions:

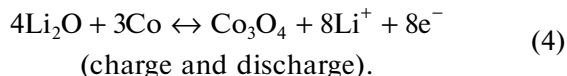
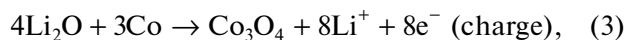
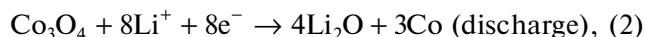


Figure 3b shows the CV curves after 200 cycles under current rate of 0.5C. The CV curves tested a total of three times of scanning. Scanning every time produce two peaks: an oxidation peak at 1.2 V and a reduction peak at 0.32 V. It's not like that the CV curve in the Fig. 3a which has a peak in 1.35 V. That is to say, the battery cycle has stabilized and there is no SEI film forming again.

The cyclic stability of the samples was investigated at a current density of 0.5C, as shown in Fig. 3c. It shows the cycling performance of the Co_3O_4 nanofibers revealing a reversible specific capacity about 300 mA h g^{-1} (calculated based on the total mass of the electrode) during the initial 200 cycles. As see from the diagram that charge specific capacity and discharge specific capacity are extraordinarily close, which show excellent coulombic efficiency of approximately 100%. It is shown that the Co_3O_4 material has

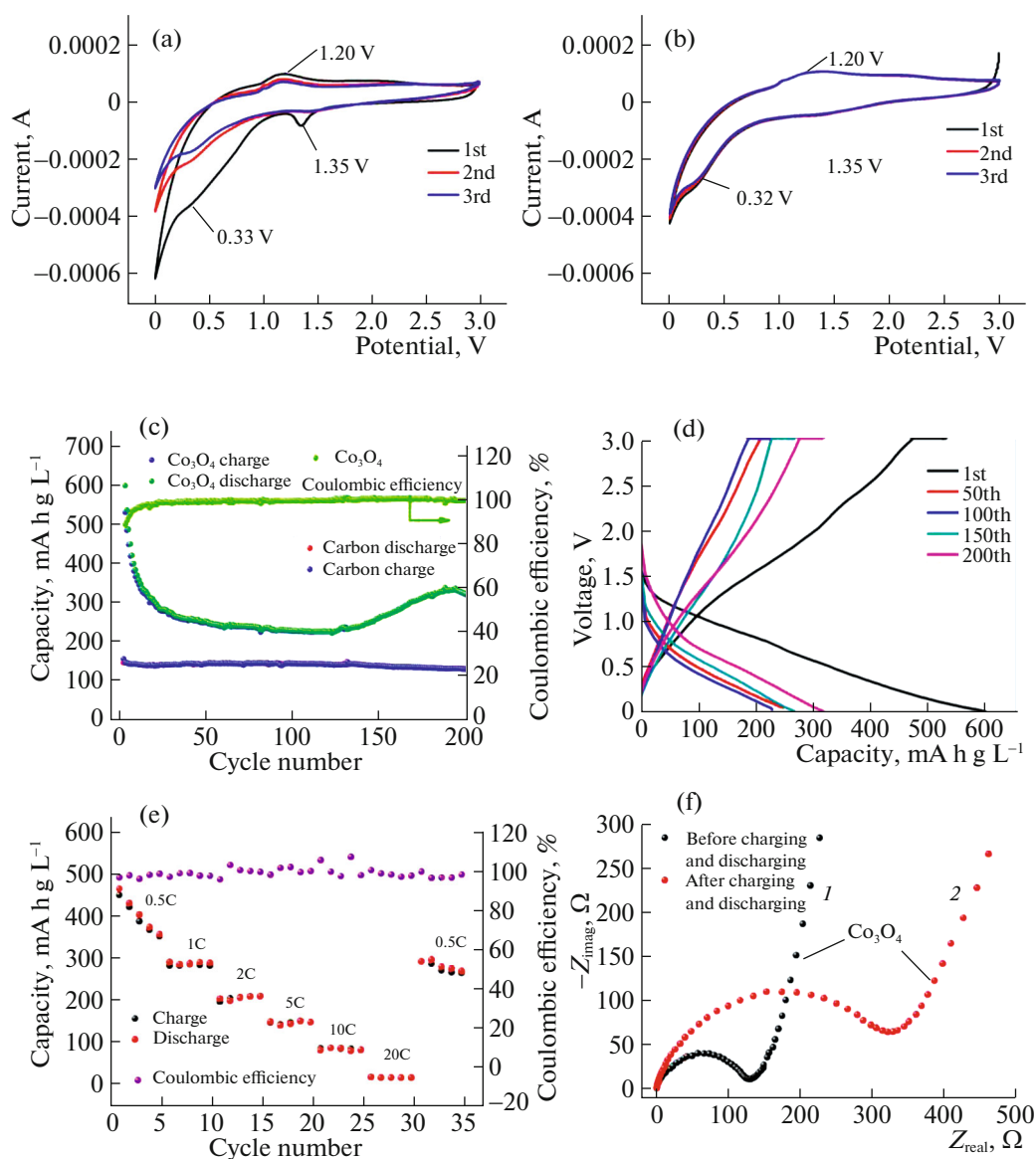


Fig. 3. (Color online) (a) The new battery CV testing of the Co_3O_4 nanofibers at the scan rate of 0.5 mVs^{-1} . (b) The CV curves after 200 cycles under the multiplying power of 0.5C. (c) The cycle efficiency and specific capacity at 0.5C current rate. (d) The galvanostatic discharge and charge curves of Co_3O_4 nanofibers for the 1st, 50th, 100th, 150th, and 200th cycles at a current rate of 0.5C. (e) The rate performance of Co_3O_4 nanofibers. (f) The Nyquist plots for Co_3O_4 nanofibers (1) at the 1st cycle and (2) after the 200 cycles at 0.5C.

good cycling performance as the anode material of lithium battery. The cyclic performance of carbon materials at the ratio of 0.5C is also shown in the Fig. 3c. However, it is obvious that Co_3O_4 materials are much better than carbon materials as anode materials for lithium-ion batteries. Although, carbon material exhibit good cyclic stability in the Fig. 3c, it is not sufficient for high energy density applications.

Figure 3d displays selected typical charge discharge profiles of Co_3O_4 measured between 0.01 and 3 V at a current density of 0.5C. There is a long steeper voltage plateau, followed by a gradually decrease until the end of the discharge. The first discharge and charge capac-

ities are 595 and 572 mA h g^{-1} based on the total mass of the composite electrode, corresponding to an irreversible capacity loss of 12%, which is probably ascribed to the formation of SEI films, some undecomposed Li_2O phase, and the irreversible decomposition of the electrolyte [27]. The rate capability of Co_3O_4 nanofibers at gradually increased current densities is shown in Fig. 3e. The Co_3O_4 exhibits good capacity retention with average discharge capacities of 368, 283, 206, 148, 87, 18, and 293 mA h g^{-1} at 0.5, 1, 2, 5, 10, 20, and 0.5C, respectively. After that, the discharge capacity recovers well to 293 mA h g^{-1} when the

current density is lowered to 0.5C. The predominant cycling and rate performances render Co_3O_4 as promising anode materials for future LIBs.

Electrochemical impedance spectroscopy (EIS) plots of the Co_3O_4 samples in the frequency range from 0.01 Hz to 100 kHz are given in Fig. 3f. All the Nyquist plots are composed of a high frequency semicircle and a slope of the straight line at low frequency, which corresponds to the charge transfer resistance on electrode and electrolyte interface, and solid-state diffusion process of lithium-ion within electrode [28]. Sample 2 is the Nyquist plots after 200 cycles. The diameter of the semicircle of sample 1 is smaller than that of sample 2, indicating that the charge transfer resistance of the sample 1 is lower, because of the formation of the SEI film in the sample 2 200 cycles at 0.5C. SEI layer decreases ion conductivity at cell storage conditions [29, 30]. The above results indicate that the Co_3O_4 nanofibers exhibits excellent reversible specific capacity and cyclic stability. The filamentous structure could accelerate Li-ion transport, as well as enhance lithium-ion mobility during the discharge/charge progress.

4. CONCLUSION

Co_3O_4 nanofibers have been successfully fabricated by electrostatic spinning. The rate performance and cycle performance show extraordinary good coulombic efficiency, approximately 100%. Electrochemical performance analysis revealed that the Co_3O_4 nanofibers provide an ideal reversible capacity about 300 mA h g^{-1} under a current density of 0.5C after 200 cycles, with better cycling performance. When the current density was increased to 0.5, 1, 2, 5, 10, 20, and 0.5C, the observed capacities were 368, 283, 206, 148, 87, 18, and 293 mA h g^{-1} , respectively. An interesting phenomenon is that the specific capacity increases after 125 cycles. This may happen because the one-dimensional structure of nanofibers provides a good channel for ion transport. These results revealed that the Co_3O_4 nanofibers are remarkable anode material for LIBs.

FUNDING

This work was financed by National Natural Science Foundation of China (11664023).

REFERENCES

1. A. Iqbal, Y. Iqbal, A. M. Khan, et al., *Russ. J. Phys. Chem. A* **91**, 2671 (2017).
2. X. J. Bai, Y. Y. Yu, H. H. Kung, et al., *J. Power Sources* **306**, 42 (2016).
3. Y. E. Roginskaya, T. L. Kulova, A. M. Skundin, et al., *Russ. J. Phys. Chem. A* **82**, 1655 (2008).
4. L. Q. Zheng, S. J. Li, D. F. Zhang, et al., *Russ. J. Phys. Chem. A* **89**, 894 (2015).
5. H. B. Wang, Q. Yu, and J. Qu, *Russ. J. Phys. Chem. A* **91**, 1152 (2017).
6. L. Q. Wu, J. Li, R. D. Deshpande, et al., *J. Phys. Chem. C* **116**, 18669 (2012).
7. M. David, G. Hugh, C. Elaine, G. Shane, L. Alex, and O. Colm, *Mater. Res. Express* **4**, 025011 (2017).
8. L. Zhan, S. Q. Wang, L. X. Ding, Z. Li, and H. H. Wang, *Electrochim. Acta* **135**, 35 (2014).
9. S. M. Abbas, S. T. Hussain, S. Ali, N. Ahmad, N. Ali, and K. S. Munawar, *Electrochim. Acta* **105**, 481 (2013).
10. H. S. Jadhav, A. K. Rai, J. Y. Lee, et al., *Electrochim. Acta* **146**, 270 (2014).
11. O. Yayapao, A. Phuruangrat, T. Thongtem, et al., *Russ. J. Phys. Chem. A* **90**, 1224 (2016).
12. L. W. Yin and Z. Li, *J. Mater. Chem. A* **3**, 21569 (2015).
13. J. F. Wu, L. Zuo, Y. H. Song, et al., *J. Alloys Compd.* **656**, 745 (2016).
14. J. M. Xu, J. S. Wu, L. L. Luo, et al., *J. Power Sources* **274**, 816 (2015).
15. L. Li, G. G. Zhou, X. Y. Shan, et al., *J. Power Sources* **255**, 52 (2014).
16. G. Carbonari, F. Maroni, M. Pasqualini, et al., *Electrochim. Acta* **247**, 392 (2017).
17. G. Huang, F. Zhang, X. Du, et al., *ACS Nano* **9**, 1592 (2015).
18. K. T. Nam, D. W. Kim, P. J. Yoo, et al., *Science (Washington, DC, U. S.)* **312**, 885 (2006).
19. W. M. Liao, J. H. Tian, Z.-Q. Shan, et al., *J. Alloys Compd.* **739**, 746 (2018).
20. Y. Jiang, X. M. Yan, W. Xiao, et al., *J. Alloys Compd.* **710**, 114 (2017).
21. G. Zhu, B. J. Jiao, and J. T. Li, *Mater. Res. Innov.* **7**, 528 (2014).
22. L. Wang, Y. Y. Fu, Y. Q. Chen, et al., *J. Alloys Compd.* **724**, 1117 (2017).
23. D. Q. Xin, J. F. Dai, J.-F. Liu, et al., *Mater. Lett.* **209**, 388 (2017).
24. Y. L. Zhang, Y. Li, J. Chen, et al., *J. Alloys Compd.* **699**, 672 (2017).
25. A. Phuruangrat, O. Yayapao, T. Thongtem, et al., *Russ. J. Phys. Chem. A* **91**, 2441 (2017).
26. Y. B. Lou, J. Liang, Y. L. Peng, et al., *Phys. Chem. Chem. Phys.* **17**, 8885 (2015).
27. G. Huang, F. F. Zhang, X. C. Du, et al., *Chem. – Eur. J.* **35**, 11214 (2014).
28. S. Sun, X. Zhao, M. Yang, et al., *Sci. Rep.* **6**, 19564 (2016).
29. A. A. Victor and W. F. Jeffrey, *J. Power Sources* **268**, 153 (2014).
30. W. Michael and S. Jeff, *J. Power Sources* **377**, 7 (2018).